

## Synthesis and Elaboration of the Dinuclear Iron-Imide Cluster Core [Fe<sub>2</sub>(μ-NR)<sub>2</sub>]<sup>2+</sup>

Jeremiah S. Duncan,<sup>†</sup> Michael J. Zdilla,<sup>†</sup> and Sonny C. Lee<sup>\*‡</sup>

Department of Chemistry, Princeton University, Princeton, New Jersey 08544, and Department of Chemistry, University of Waterloo, Waterloo, Ontario, Canada N2L 3G1

Received June 22, 2006

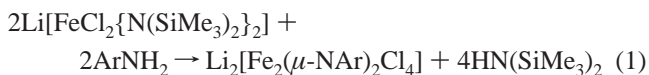
The protolysis of mononuclear ferric amide precursors FeCl[N(SiMe<sub>3</sub>)<sub>2</sub>]<sub>2</sub>(THF) (**1**) or [FeCl<sub>2</sub>{N(SiMe<sub>3</sub>)<sub>2</sub>]<sub>2</sub>]<sup>-</sup> (**2**) by primary amines provides, under suitable conditions, an effective route to dinuclear weak-field ferric-imide clusters with [Fe<sub>2</sub>(μ-NR)<sub>2</sub>]<sup>2+</sup> cores. In the synthesis of known arylimide clusters [Fe<sub>2</sub>(μ-NAr)<sub>2</sub>Cl<sub>4</sub>]<sup>2-</sup> (Ar = Ph, *p*-Tol, Mes) from **2**, the counterion has a major effect on selectivity and yield, and the use of quaternary ammonium salts affords a substantial improvement over earlier, Li<sup>+</sup>-based chemistry. The new *tert*-butylimide core is obtained by protolysis of **1** with excess <sup>t</sup>BuNH<sub>2</sub> to give crystalline *cis*-Fe<sub>2</sub>(μ-N<sup>t</sup>Bu)<sub>2</sub>Cl<sub>2</sub>(NH<sub>2</sub><sup>t</sup>Bu)<sub>2</sub> (**9**). Complex **9** can be transformed to other dinuclear species through substitution of the terminal amines by pyridines, PEt<sub>3</sub>, or chloride, or through protolysis of bridging alkylimides by arylamines, allowing isolation of *trans*-Fe<sub>2</sub>(μ-N<sup>t</sup>Bu)<sub>2</sub>Cl<sub>2</sub>(DMAP)<sub>2</sub> (DMAP = 4-dimethylaminopyridine), *cis*-Fe<sub>2</sub>(μ-N<sup>t</sup>Bu)<sub>2</sub>Cl<sub>2</sub>(PEt<sub>3</sub>)<sub>2</sub>, [Fe<sub>2</sub>(μ-N<sup>t</sup>Bu)<sub>2</sub>Cl<sub>4</sub>]<sup>-</sup>, and *trans*-Fe<sub>2</sub>(μ-NPh)<sub>2</sub>Cl<sub>2</sub>(NH<sub>2</sub><sup>t</sup>Bu)<sub>2</sub>. The susceptibility of alkyl substituents to β-elimination appears to limit the general applicability of protolytic cluster assembly using alkylamines. The dinuclear clusters have been characterized by X-ray, spectroscopic, and electrochemical analyses.

### Introduction

Clusters of weak-field iron with imide core ligation constitute a relatively new class of inorganic compounds.<sup>1–4</sup> The iron-imide (Fe–NR) environment offers several points of interest: the metal–ligand combination is markedly different from those found in other existent cluster types; the resulting chemistry is likewise novel and has led, for example, to the isolation of stable iron complexes in high-valent states and with terminal imide coordination;<sup>2,3</sup> and the interaction of weak-field iron and nitrogen anions suggests a chemical connection to current understanding and speculation regarding biological nitrogen fixation.<sup>3,5,6</sup> Initial studies point to the existence of an extensive Fe–NR chemistry,

comparable in scope to that observed in the well-known iron-sulfur systems.<sup>3,6</sup>

The exploration of this chemistry requires the systematic development of general synthetic routes to Fe–NR species. We have reported one such avenue to Fe–NR cluster assembly, involving the protolysis of ferric bis(amide) precursors, FeCl[N(SiMe<sub>3</sub>)<sub>2</sub>]<sub>2</sub>(THF) (**1**) or [FeCl<sub>2</sub>{N(SiMe<sub>3</sub>)<sub>2</sub>]<sub>2</sub>]<sup>-</sup> (**2**), by primary arylamines (ArNH<sub>2</sub>).<sup>3</sup> A balanced prototype reaction leading to the formation of a simple dinuclear Fe–NR cluster (**3**) is given as eq 1.



In practice, the outcomes of these protolysis reactions were complicated by redox activity at both metal and amine and by the simultaneous formation of several different cluster products.<sup>3</sup> The reaction envisaged in eq 1, when applied to Ar = Ph, actually yields not only the indicated diferric [Fe<sub>2</sub>(μ-NPh)<sub>2</sub>Cl<sub>4</sub>]<sup>2-</sup> cluster (**3a**) but also an oxidized (relative to the ferric starting complex) trinuclear cluster, [Fe<sub>3</sub>(μ-NPh)<sub>4</sub>Cl<sub>4</sub>]<sup>2-</sup> (**4a**), in an approximately equimolar amount, as well as a reduced tetranuclear heterocubane cluster, [Fe<sub>4</sub>(μ<sub>3</sub>-NPh)<sub>4</sub>Cl<sub>4</sub>]<sup>2-</sup> (**5a**), as a minor product. Although this

\* To whom correspondence should be addressed. E-mail: scllee@uwaterloo.ca.

<sup>†</sup> Princeton University.

<sup>‡</sup> University of Waterloo.

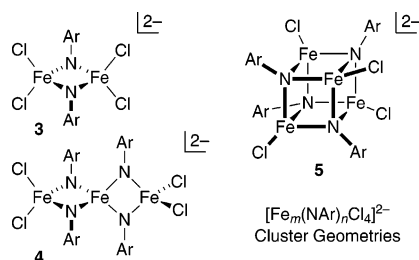
- (1) Verma, A. K.; Lee, S. C. *J. Am. Chem. Soc.* **1999**, *121*, 10838.
- (2) Verma, A. K.; Nazif, T. M.; Achim, C.; Lee, S. C. *J. Am. Chem. Soc.* **2000**, *122*, 11013.
- (3) Duncan, J. S.; Nazif, T. M.; Verma, A. K.; Lee, S. C. *Inorg. Chem.* **2003**, *42*, 1211.
- (4) (a) Link, H.; Decker, A.; Fenske, D. Z. *Anorg. Allg. Chem.* **2000**, *626*, 1567. (b) Link, H.; Reiss, P.; Chitsaz, S.; Pfister, H.; Fenske, D. Z. *Anorg. Allg. Chem.* **2003**, *629*, 755.
- (5) Lee, S. C.; Holm, R. H. *Proc. Natl. Acad. Sci. U.S.A.* **2003**, *100*, 3595.
- (6) Lee, S. C.; Holm, R. H. *Chem. Rev.* **2004**, *104*, 1135.

**Chart 1.** Compound Designations<sup>a</sup>

FeCl[N(SiMe <sub>3</sub> ) <sub>2</sub> ] <sub>2</sub> (THF)	1
[FeCl <sub>2</sub> {N(SiMe <sub>3</sub> ) <sub>2</sub> }]	2
[Fe <sub>2</sub> (μ-NAr) <sub>2</sub> Cl <sub>4</sub> ] <sup>2-</sup>	3a (Ar = Ph), 3b (Ar = <i>p</i> -Tol), 3c (Ar = Mes)
[Fe <sub>3</sub> (μ <sub>3</sub> -NPh) <sub>4</sub> Cl <sub>4</sub> ] <sup>2-</sup>	4a
[Fe <sub>3</sub> (μ <sub>3</sub> -NPh) <sub>4</sub> Cl <sub>4</sub> ] <sup>-</sup>	5a
[Fe <sub>4</sub> (μ <sub>3</sub> -N <sup><i>t</i></sup> Bu) <sub>4</sub> Cl <sub>4</sub> ] <sup>-</sup>	6 (z = 0), 7 (z = 1-)
[Fe <sub>2</sub> (μ-N <sup><i>t</i></sup> Bu) <sub>2</sub> Cl <sub>4</sub> ] <sup>2-</sup>	8
Fe <sub>2</sub> (μ-N <sup><i>t</i></sup> Bu) <sub>2</sub> Cl <sub>2</sub> L <sub>2</sub>	9 (L = <sup><i>t</i></sup> BuNH <sub>2</sub> ), 10 (L = DMAP), 11 (L = PEt <sub>3</sub> )
Fe <sub>2</sub> (μ-NPh) <sub>2</sub> Cl <sub>2</sub> (NH <sub>2</sub> <sup><i>t</i></sup> Bu) <sub>2</sub>	12

<sup>a</sup> Abbreviations: THF = tetrahydrofuran; *p*-Tol = *para*-tolyl; Mes = mesityl; DMAP = 4-dimethylaminopyridine.

chemistry is workable for the synthesis of Fe–NR clusters, tuning of crystallization conditions or aryl substituent sterics on a specific case basis is necessary for the isolation of pure clusters.

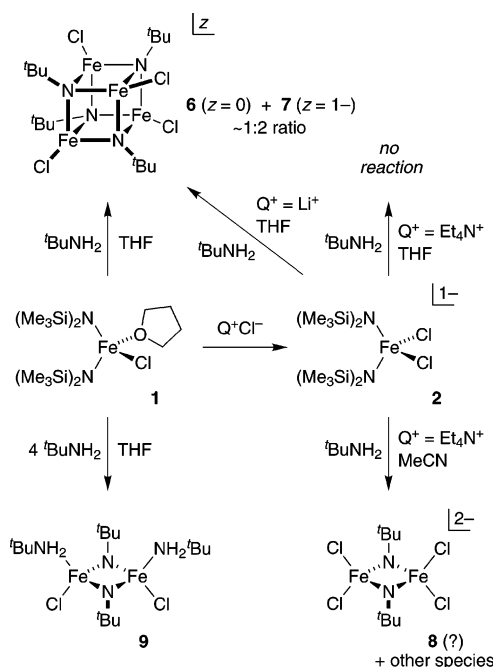


We report here a further study of this protolysis-induced cluster assembly system and its extension to the use of alkylamines as imide sources as well as a first survey of the reaction chemistry of a dinuclear Fe–NR cluster. The synthetic modifications presented in this account provide substantially improved access to known and new diferric diimide clusters.

## Results and Discussion

A complete index of compounds discussed in the following sections is provided as Chart 1.

**ArNH<sub>2</sub> Protolysis: Influence of Counterion on Cluster Assembly.** The choice of Li<sup>+</sup> as counterion in the original protolysis system<sup>3</sup> (e.g., eq 1) arose from concerns regarding the stability of Fe–NR species toward organic cations and the polar solvents typically used in their manipulation. Ferrous amides, for example, decompose within minutes in MeCN, and the highly basic lithium salts of amides and imides are much more reactive still. We have found, however, that amide and imide species bound to oxidized iron (with mean oxidation states tending toward ferric) are in fact fairly robust and reasonably stable in polar organic environments, provided that dioxygen and moisture are rigorously excluded. Given that Li<sup>+</sup> can be problematic for the isolation of Fe–NR salts due to contamination from LiCl and desolvation/decomposition involving solvated lattice cations in the solid state, we investigated the substitution of quaternary ammonium cations (R<sub>4</sub>N<sup>+</sup>) for Li<sup>+</sup> in this system.

**Scheme 1**

The reaction of complex **1** with (R<sub>4</sub>N)Cl (R = Et, *n*-Bu) in MeCN or THF leads to a transparent orange-red solution color indicative of the formation of the known chloride adduct **2** (eq 2).<sup>3</sup> The crystalline Et<sub>4</sub>N<sup>+</sup> salt of anion **2** can be obtained in high yield using THF as the reaction medium,<sup>7</sup> operationally, however, it is easier and just as effective to generate **2** in situ for one-pot reactions.



Addition of ArNH<sub>2</sub> to solutions containing [R<sub>4</sub>N]**2** indeed results in the formation of Fe–NR clusters. Unlike the analogous reaction with Li<sup>+</sup> as counterion,<sup>3</sup> the use of quaternary ammonium cations gives the precise stoichiometric chemistry formulated in eqs 2 and 3, affording dinuclear Fe–NR species **3** with excellent selectivity (typically >90% of the cluster products in the crude reaction solution, by <sup>1</sup>H NMR assay) and high isolated yields (>80% in optimized cases). We have tested this reaction with amine Ar = Ph (**3a**), *p*-Tol (**3b**), Mes (**3c**), and ammonium R = Et, *n*-Bu, and in MeCN and THF solvents (the dianionic clusters are soluble in the former, but precipitate directly and copiously from the latter); the product selectivity is essentially the same throughout. Thus, this simple change in counterion provides a useful, and likely general, route to [Fe<sub>2</sub>(μ-NAr)<sub>2</sub>Cl<sub>4</sub>]<sup>2-</sup> clusters.

(7) [Et<sub>4</sub>N]**2** was definitively identified by single-crystal X-ray diffraction analysis; the structure of the anion does not differ significantly from that previously reported for the [Li(TMEDA)<sub>2</sub>]<sup>+</sup> salt.<sup>3</sup> Essential crystal data are listed in Table 4, with structural details available as Supporting Information.

The relationship between counterion and reaction outcome is somewhat surprising inasmuch as the choice of counterion is not usually considered a determinative parameter for cluster assembly in solution.<sup>8</sup> We speculate that, in this reaction system, the counterion can affect ligand lability at iron: the accessible, concentrated charge density at  $\text{Li}^+$  allows for direct interactions at basic ligand sites (chloride, amide, or imide donor atoms) relative to shielded quaternary ammonium cations; this labilizes bound chloride and/or weakens amide or imide bridging as a result, thereby altering cluster formation pathways. Other observations support this hypothesis: (1) Cation-induced terminal ligand labilization ( $\text{Na}^+$  vs  $\text{R}_4\text{N}^+$ , in this instance) has been found and quantified in  $[\text{Fe}_4\text{S}_4]^{2+}$  clusters.<sup>9</sup> (2) Direct interactions between  $\text{Li}^+$  and terminal chloride ligands have been observed in the solid state for iron arylimide clusters, e.g.,  $[\text{Li}(\text{THF})_4][\text{Li}(\text{THF})_3][\text{Fe}_2(\mu\text{-NMe}_2)_2\text{Cl}_4]$ ,<sup>3</sup>  $[\text{Li}(\text{THF})_2]_2[\text{Fe}_2(\mu\text{-NMe}_2)_2\text{Cl}_4]$ ,<sup>4a</sup> and  $[\text{Li}(\text{THF})_4][\text{Li}(\text{THF})_3][\text{Fe}_4(\mu_3\text{-NPh})_4\text{Cl}_4]$ .<sup>4a</sup> (3) The addition of a  $\text{Li}^+$  source with a weakly coordinating counteranion ( $\text{LiClO}_4$ ) to solutions of pure  $[\text{Et}_4\text{N}]\mathbf{3a}$  gives rise to clusters **4a** and **5a** in limited quantities after 24 h; solutions of  $[\text{Et}_4\text{N}]\mathbf{3a}$  without  $\text{Li}^+$  are stable over this time course, suggesting that  $\text{Li}^+$  triggers cluster rearrangements.

We note that the rate of protolytic cluster assembly (eqs 1 and 3), as qualitatively gauged by solution color changes, is a complicated function of both counterion and solvent: under equivalent conditions, reaction rates order as  $\text{Li}^+$ ,  $\text{Et}_4\text{N}^+ > (n\text{-Bu}_4\text{N})^+$  (mins vs days); for  $\text{Li}^+$ ,  $\text{MeCN} > \text{THF}$  ( $\sim 1$  min vs  $\sim 10$  min); for  $\text{Et}_4\text{N}^+$ ,  $\text{THF} > \text{MeCN}$  ( $\sim 1$  min vs  $\sim 10$  min); and for  $n\text{-Bu}_4\text{N}^+$ ,  $\text{MeCN} > \text{THF}$  ( $\sim 1$  day vs several days). Although we cannot offer a simple mechanistic rationalization for these observations, it seems clear that ion solvation and/or solvent ligation influence reactivity in this system.

**Protolysis by  $t\text{-BuNH}_2$ .** At first glance, the extension of the protolytic cluster assembly chemistry to alkylamines might seem unpromising due to their substantially reduced acidity relative to silyl- and arylamines.<sup>10</sup> Protolysis can proceed nonetheless, albeit at much reduced rates of minutes-to-hours for alkylamine protolysis vs seconds-to-minutes for arylamines. The property differences between aryl- and alkylamines lead to further, significant changes in the chemistry, as described below.

Following our experience in arylamine protolysis,<sup>3</sup> we first evaluated the minimal two-component reaction system of complex **1** and primary alkylamine. Alkylamines with primary or secondary substituents ( $\text{PhCH}_2\text{NH}_2$ ,  $n\text{-BuNH}_2$ ,  $i\text{-PrNH}_2$ ) react with 1 equiv of complex **1** to give deep brown-black solutions, but generate neither NMR-detectable paramagnetic solution species nor well-defined solid products. Aqueous acidification of the dark material obtained

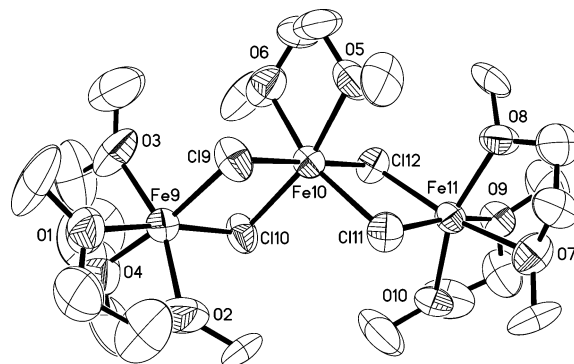
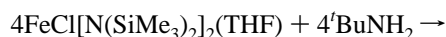


**Figure 1.** Cation structure of  $[\text{Fe}_3(\mu\text{-Cl})_4(\text{DME})_5][\text{Fe}_4(\mu_3\text{-N}^t\text{Bu})_4\text{Cl}_4]_2\cdot\text{DME}$  ( $[\text{Fe}_3(\mu\text{-Cl})_4(\text{DME})_5][\mathbf{7}]_2\cdot\text{DME}$ ) with thermal ellipsoids (35% probability level) and selected atom labels. Hydrogen atoms are not shown. Selected distance ranges [mean] (Å): Fe–O, 2.121(11)–2.210(13) [2.16(3)]; Fe–Cl, 2.385(5)–2.493(4) [2.43(4)];  $\text{Fe}\cdots\text{Fe}$ , 3.504(3), 3.512(3) [3.508(6)]. Details for the structure of the known<sup>2,4a</sup> heterocubane cluster anion are provided as Supporting Information.<sup>13</sup>

from the reaction of **1** with benzylamine, followed by extractive workup and GC analysis, reveals benzaldehyde in 16% recovered yield, a hydrolysis product expected if  $\beta$ -elimination occurs to form benzylimine (or iron-coordinated benzyliminide).

Attention was therefore directed to synthesis using an alkylamine unsusceptible to  $\beta$ -elimination, as outlined in Scheme 1. When complex **1** is treated with 1 equiv of  $t\text{-BuNH}_2$  in THF,<sup>11</sup> the known heterocubane clusters  $\text{Fe}_4(\mu_3\text{-N}^t\text{Bu})_4\text{Cl}_4$  (**6**) and  $[\text{Fe}_4(\mu_3\text{-N}^t\text{Bu})_4\text{Cl}_4]^-$  (**7**)<sup>2,4a</sup> form in a ca. 1:2 ratio as the principal<sup>12</sup> Fe–NR products by  $^1\text{H}$  NMR analysis. Anion **7** is accompanied by NMR-silent cationic chloroferrous species, as demonstrated by the crystallization of  $[\text{Fe}_3(\mu\text{-Cl})_4(\text{DME})_5][\mathbf{7}]_2$  from concentrated dimethoxyethane (DME) solutions.<sup>13</sup> The trinuclear counterion, constructed as a chloride-bridged, edge-shared, bent trioctahedron with idealized  $C_2$  symmetry (Figure 1), is new to our knowledge; its assignment as an all-ferrous dication derives from the  $^1\text{H}$  NMR identification of **7**.<sup>14</sup>



While the formation of neutral **6** is exact for simple protolysis (eq 4), the predominant production of both reduced cluster **7** and its ferrous counterion implicates the intervention of additional, redox-based chemistry, presumably in the form of Fe(III) reduction coupled to amine oxidation. Similar behavior was documented in aniline protolysis,<sup>3</sup> although in

(8) We confine this discussion strictly to solution behavior, excluding situations where counterion-dependent precipitation/crystallization properties affect the cluster product isolated.

(9) Henderson, R. A. *J. Chem. Soc., Dalton Trans.* **1999**, 119.

(10) (a) Comparative  $\text{p}K_a$  values in DMSO:  $\text{PhNH}_2$ , 30.6; Bordwell, F. G. *Acc. Chem. Res.* **1988**, *21*, 456. (b) In THF:  $i\text{-PrNH}_2$ , 35.7;  $(\text{Me}_3\text{Si})_2\text{NH}$ , 25.8; Fraser, R. R.; Mansour, T. S. *J. Org. Chem.* **1984**, *49*, 3443. Also, see correction: *J. Org. Chem.* **1984**, *49*, 5284.

(11) If MeCN is used as the solvent instead of THF, the reaction rapidly ( $< 10$  s) generates insoluble material; this precipitate dissolves upon addition of  $\text{LiCl}$  or  $(\text{Et}_4\text{N})\text{Cl}$  to give as yet unidentified NMR-detectable species.

(12) Other paramagnetic cluster species, including the terminal-imide containing heterocubane  $\text{Fe}_4(\text{N}^t\text{Bu})_5\text{Cl}_3$ ,<sup>2</sup> are also observed as minor coproducts.

(13)  $[\text{Fe}_3(\mu\text{-Cl})_4(\text{DME})_5][\mathbf{7}]_2$  was characterized by single-crystal X-ray diffraction analysis; the structure of the heterocubane anions are almost indistinguishable from those previously reported in  $\text{Li}^+$  salts.<sup>2,4a</sup> Essential crystal data are listed in Table 4, with structural details available as Supporting Information.

(14)  $^1\text{H}$  NMR ( $\text{CD}_3\text{CN}$ , 25 °C)  $\delta$  11.44 ( $t\text{-Bu}$ ). Duncan, J. S.; Zdilla, M. J.; Lee, S. C. Manuscript in preparation.

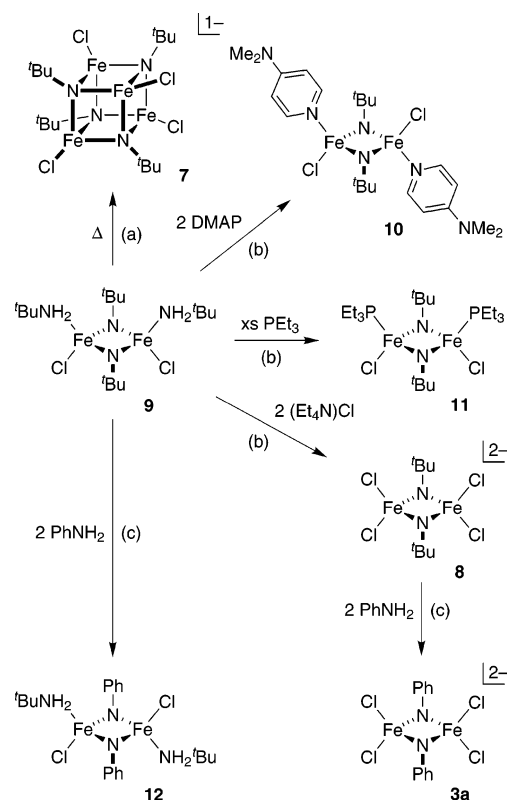
that system, the chloroferrous cations are associated with linear trinuclear cluster **4a** as the Fe–NR product, with no indication of heterocubane species; the greater nitrogen basicity<sup>15</sup> of alkylamines relative to arylamines may explain the  $\mu_3$ -bridging in the present situation. In both cases, this redox chemistry is detrimental for preparative purposes. The substitution of the anionic chloride-adduct **2** for complex **1** was effective in controlling redox chemistry during arylamine protolysis<sup>3</sup> (subject to counterion effects, *vide supra*), and this approach was pursued here.

The protolysis of [Li]**2** by <sup>t</sup>BuNH<sub>2</sub> in THF (per eq 1) is markedly slower than the equivalent reaction with **1** (ca. 1 day vs 15 min), presumably reflecting competition between chloride and amine coordination, but the product outcome is unchanged. When [Et<sub>4</sub>N]**2** is used instead (per eq 3), the effect on reaction rate is extreme, with virtually no cluster formation even after several days; this provides additional, dramatic evidence for cation-dependent ligand lability. If this last reaction is conducted in MeCN, the stoichiometric [Fe<sub>2</sub>( $\mu$ -N<sup>t</sup>Bu)<sub>2</sub>Cl<sub>4</sub>]<sup>2-</sup> target (**8**) does seem to form, as judged by <sup>1</sup>H NMR comparison with authentic sample (*vide infra*); the high-polarity MeCN solvent may allow cluster assembly to proceed by facilitating dissociation of ligated chloride. The reaction in MeCN, however, also generates other, unknown paramagnetic products that prevented the isolation of **8** from this system. In contrast to the arylamine chemistry, the protolysis of **2** by <sup>t</sup>BuNH<sub>2</sub> proved surprisingly ineffective for cluster synthesis.

Ultimately, a simple modification of the original two-component reaction system allowed access to a dinuclear cluster product in useful quantities. The reaction of 4 equiv of <sup>t</sup>BuNH<sub>2</sub> with complex **1** in THF affords a red-brown solution, from which a rust-red solid is obtained after solvent removal and pentane washes. This material is insoluble in hydrocarbon solvents but can be recrystallized from THF/pentane to give pure, crystalline Fe<sub>2</sub>( $\mu$ -N<sup>t</sup>Bu)<sub>2</sub>Cl<sub>2</sub>(NH<sub>2</sub><sup>t</sup>Bu)<sub>2</sub> (**9**) as the *cis* isomer in good yield. In CD<sub>3</sub>CN solution, **9** presents two broad, isotropically shifted, equal intensity <sup>1</sup>H NMR resonances. This pattern fits the solid-state structure, with separate <sup>t</sup>Bu signals for the bridging imides and the terminal amines; the peak furthest downfield can be assigned to the imide by comparison with the spectrum of the all-chloride derivative **8**. To our knowledge, cluster **9** and its derivatives (*vide infra*) contain the first examples of  $\mu_2$ -alkylimide bridging at iron.

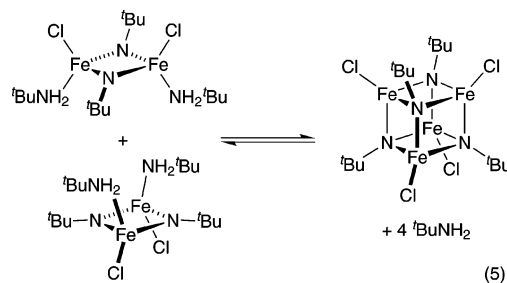
**Stability and Reactivity of Fe<sub>2</sub>( $\mu$ -N<sup>t</sup>Bu)<sub>2</sub>Cl<sub>2</sub>(NH<sub>2</sub><sup>t</sup>Bu)<sub>2</sub> (**9**).** The isolation of **9** suggests that excess <sup>t</sup>BuNH<sub>2</sub> affects cluster assembly by competing for available coordination sites, thereby suppressing aggregation past the dinuclear stage. The affinity of <sup>t</sup>BuNH<sub>2</sub> for labile iron centers and its effect on cluster assembly was unanticipated, as amines occur infrequently as monodentate ligands on iron, and never previously, in monodentate or chelate form, at 4-coordinate Fe(III) sites.<sup>16</sup> This, in conjunction with other distinctive

Scheme 2



aspects of the coordination environment, raised specific questions regarding the stability and reactivity of **9**.

**(a) Is **9** Metastable in Solution?** From similarities in structure and synthesis, it is tempting to relate dinuclear **9** and heterocubane **6** through a simple fusion/fission equilibrium (eq 5). Solutions of **9**, however, are stable for days at room temperature and show no heterocubane formation by <sup>1</sup>H NMR assay; likewise, solutions of hetero-



cubane evince no reaction with excess <sup>t</sup>BuNH<sub>2</sub>. Heating of **9** at 85 °C for several hours does yield the heterocubane, but as the reduced cluster **7** (Scheme 2a); heterocubane assembly in this instance appears more complicated than just amine loss followed by condensation of dinuclear fragments, and other, undetected species (e.g., amine oxidation products, reduced iron (ferrous) cations, [<sup>t</sup>BuNH<sub>3</sub>]<sup>+</sup>) must also be formed.

**(b) Given the Apparent Stability of **9**, What Is the Lability of the Coordinated Amines?** <sup>1</sup>H NMR titration of **9** (20 mM in CD<sub>3</sub>CN) with <sup>t</sup>BuNH<sub>2</sub> (up to 8 equiv) leads to limited broadening of the bound amine resonance, along with the appearance and growth of a very broad peak with a chemical shift indicative of free amine. Intermolecular

(15) Comparative pK<sub>a</sub> values in DMSO (H<sub>2</sub>O): [PhNH<sub>3</sub>]<sup>+</sup>, 3.6 (4.6); [NH<sub>4</sub>]<sup>+</sup>, 10.5 (9.2).<sup>10a</sup>

(16) Cambridge Structural Database, version 5.26. Allen, F. H. *Acta Crystallogr.* **2002**, B58, 380.

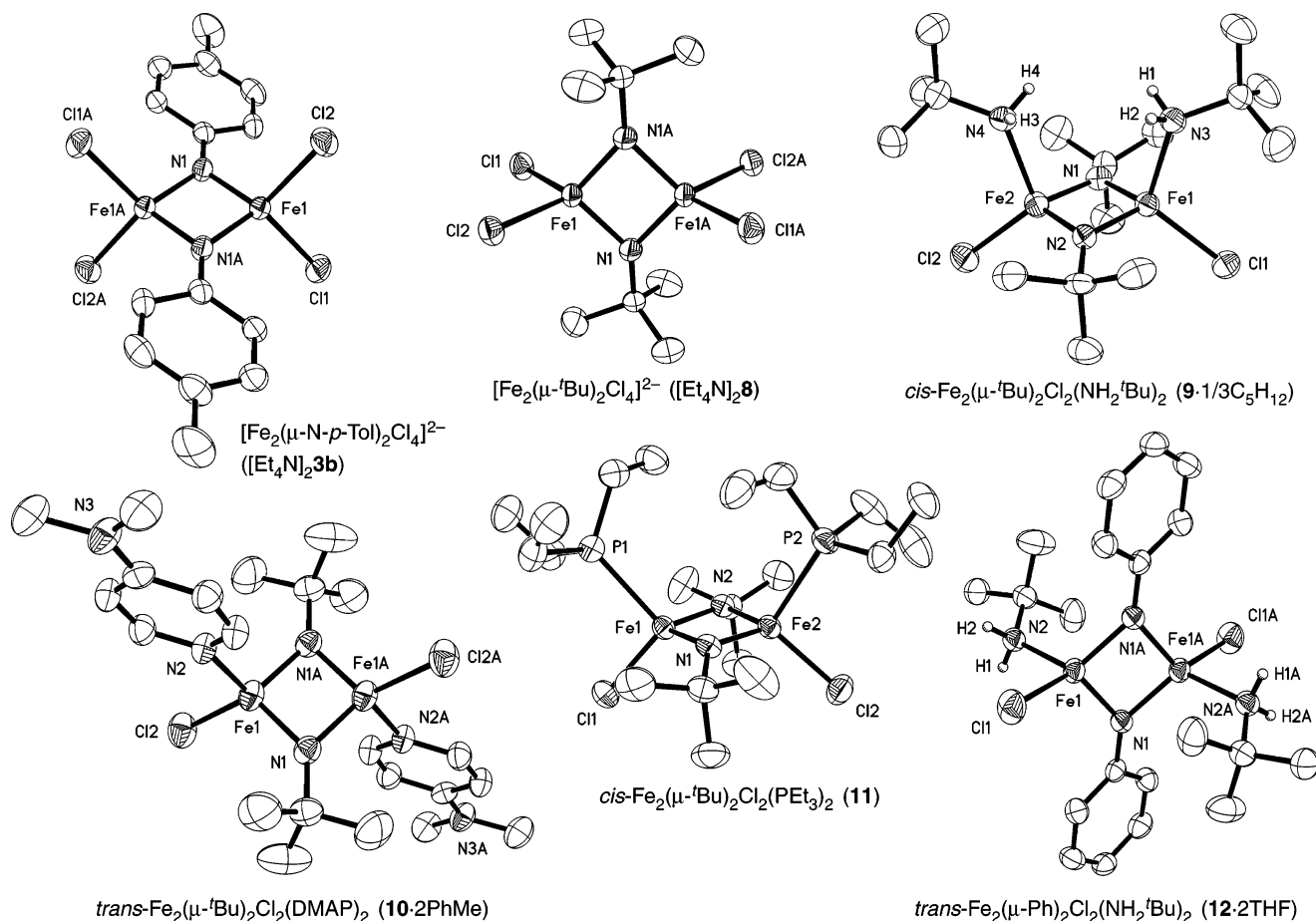


**Figure 2.** Dinuclear Fe–NR cluster structures with thermal ellipsoids (50% probability level) and selected atom labels. Hydrogen atoms are not shown, except for the amine hydrogens in **9** and **12**, which were located and refined. Atoms with labels ending in “A” are generated by crystallographic inversion symmetry. The structures of the arylimide clusters in  $[\text{Et}_4\text{N}]_2\mathbf{3a}$  and  $[n\text{-Bu}_4\text{N}]_2\mathbf{3c}$  are nearly indistinguishable from those in equivalent  $\text{Li}^+$  salts reported previously<sup>3,4a</sup> and are not shown here.

exchange of amine under these conditions is therefore slow at best on the spectroscopic timescale (500 MHz, 25 °C).

Amine lability was demonstrated by ligand substitution (Scheme 2b). Addition of 2 equiv of  $(\text{Et}_4\text{N})\text{Cl}$  to THF or MeCN solutions of **9** cleanly gives, in high isolated yield, the all-chloride dimer **8**, which was previously unattainable in pure form by direct protolysis. The choice of counterion is again important: the use of  $\text{LiCl}$  instead of  $(\text{Et}_4\text{N})\text{Cl}$  gives a product mixture that includes multiple dinuclear species and heterocubanes, as ascertained by  $^1\text{H}$  NMR spectroscopy and crystallographic structure determinations.

The coordinated amines can also be displaced by neutral donors (Scheme 2b), although the chemistry is less straightforward. Thus, dissolution of **9** in pyridine- $d_5$  produces a  $^1\text{H}$  NMR spectrum with a broad imide resonance (positioned slightly upfield of the equivalent signal in **9**) and sharp signals corresponding to free  $t\text{BuNH}_2$ , consistent with displacement of the bound amines by pyridine with retention of the  $[\text{Fe}_2(\mu\text{-N}^t\text{Bu})_2]^{2+}$  core structure. Although we were unable to isolate the pyridine-substituted product, we were able to identify a 4-dimethylaminopyridine (DMAP) derivative, prepared from the reaction of **9** with 2 equiv of DMAP, as the trans adduct  $\text{Fe}_2(\mu\text{-N}^t\text{Bu})_2\text{Cl}_2(\text{DMAP})_2$  (**10**) by structural analysis. A more detailed characterization of **10** is complicated by side reactions and solution instability (evident

in its  $^1\text{H}$  NMR spectrum and in difficulties with recrystallization), and pure material was unavailable in useful quantities. Triethylphosphine ( $\text{PET}_3$ ) can also replace the coordinated amine in **9**, giving cis-oriented  $\text{Fe}_2(\mu\text{-N}^t\text{Bu})_2\text{Cl}_2(\text{PET}_3)_2$  (**11**) in good crystalline yield. Excess phosphine is imperative for good conversion: at 10 mM of **9** and 8 equiv of  $\text{PET}_3$ ,  $^1\text{H}$  NMR analysis of the equilibrium solution reveals the presence of residual **9**.

**(c) Are the Bridging Imides Reactive?** We have previously found that the triply bridging arylimides in  $[\text{Fe}_4(\mu_3\text{-NAr})_4]^{4+}$  heterocubane cores readily undergo protolytic exchange.<sup>1</sup> This behavior exists for the  $\mu_2$ -alkylimides in the current clusters as well, where  $\text{p}K_a$  differences<sup>10</sup> can be exploited to replace bridging alkylimides with arylimides (Scheme 2c). Thus, the reaction of **9** with 2 equiv of aniline gives  $\text{Fe}_2(\mu\text{-NPh})_2\text{Cl}_2(\text{NH}_2^t\text{Bu})_2$  (**12**) in good yield; the new, core-substituted product retains the terminal ligand composition of the starting cluster, albeit with a trans geometry in the solid state. Likewise, complex **8** reacts smoothly with aniline (2 equiv) to give phenylimide cluster **3a** as the sole, quantitative product by  $^1\text{H}$  NMR analysis.

**(d) How Stable Are Mixed Terminal Donor Environments?** We would expect clusters composed of high-spin, exchange-labile metal sites and mixed (differentiated) monodentate terminal ligand sets to be prone to facile redistribution

**Table 1.** Selected Structural Metrics for Dinuclear Fe–NR Clusters<sup>a</sup>

(L =)	<b>3a</b>	<b>3b</b>	<b>3c</b>	<b>8</b>	<b>9</b> (tBuNH <sub>2</sub> )	<b>10</b> (DMAP)	<b>11</b> (PEt <sub>3</sub> )	<b>12</b> (tBuNH <sub>2</sub> )
				Distances <sup>b</sup> (Å)				
Fe–N <sub>b</sub>	1.881(2)	1.882(6)	1.872(3)	1.864(2)	1.860(6)	1.853(4)	1.861(5)	1.877(2)
Fe–Cl	2.2719(8)	2.271(5)	2.285(7)	2.31(2)	2.254(1)	2.2550(15)	2.247(8)	2.2586(11)
Fe–L					2.16(1)	2.094(4)	2.47(2)	2.106(3)
Fe···Fe	2.5656(11)	2.5667(8)	2.5270(11)	2.5080(12)	2.4769(9)	2.4791(14)	2.4758(7)	2.5354(10)
N <sub>b</sub> ···N <sub>b</sub>	2.752(5)	2.753(5)	2.762(6)	2.757(7)	2.773(5)	2.755(8)	2.777(4)	2.768(5)
				Angles <sup>b</sup> (deg)				
N <sub>b</sub> –Fe–N <sub>b</sub>	94.02(12)	94.00(11)	95.08(13)	95.41(14)	96.4(4)	96.0(2)	96.5(2)	95.01(10)
Cl–Fe–N <sub>b</sub>	114(2)	114.2(6)	114(2)	115(2)	120(2)	119.2(9)	119(1)	120(2)
L–Fe–N <sub>b</sub>					102(2)	106.9(6)	112(4)	112(2)
(Cl/L)–Fe–Cl	105.50(4)	106.24(3)	105.09(5)	101.71(5)	112.6(3)	107.53(11)	100(3)	98.69(9)
Fe–N <sub>b</sub> –Fe	85.98(12)	86.00(11)	84.92(13)	84.59(14)	83.5(2)	84.0(2)	83.4(3)	84.98(10)
				Planarity <sup>b</sup> (Å) or Torsion <sup>b</sup> (deg)				
Fe <sub>2</sub> (μ–N <sub>b</sub> ) <sub>2</sub> <sup>c</sup>	0	0	0	0	0.024(1)	0	0.028(1)	0
N <sub>b</sub> <sup>d</sup>	0.061(3)	0.009(3)	0.017(4)	0.081(4)	0.14(2)	0.036(5)	0.26(1)	0.0002(3)
N <sub>b</sub> –Ar <sup>e</sup>	7.02(10)	16.47(15)	89.74(9)					

<sup>a</sup> Italicized entries are averaged values corresponding to clusters with idealized  $D_{2d}$  (**3a–c**, **8**),  $C_{2v}$  (**9**, **11**), or  $C_{2h}$  (**10**, **12**) symmetries. <sup>b</sup> N<sub>b</sub> refers to bridging imide nitrogen atoms. <sup>c</sup> RMS deviation from the least-squares-fitted [Fe<sub>2</sub>N<sub>2</sub>] rhomb plane. <sup>d</sup> Nitrogen pyramidalization as measured by the perpendicular displacement from the plane of the directly bonded atoms [Fe, Fe', C<sup>a</sup>]. <sup>e</sup> Dihedral angle between the least-squares-fitted [Fe<sub>2</sub>N<sub>2</sub>] rhomb and aryl ring planes.

in solution. The <sup>1</sup>H NMR spectrum of crystalline, analytically pure **11** shows evidence of this behavior, in the form of resonances in excess of those predicted from the solid-state structure. In contrast, *tert*-butylamine-ligated clusters **9** and **12** present NMR signatures in complete agreement with their crystallographically determined structures. This differential stability, in conjunction with other, aforementioned solution properties, may reflect a higher affinity for alkylamine relative to phosphine or pyridine ligation in these clusters.

It is curious that the <sup>1</sup>H NMR data for both **9** and **12** seemingly show the existence of just one stereochemistry in solution. We discern no obvious physical basis for their respective terminal ligand dispositions other than crystal packing. Given the lability of tetrahedral Fe(III), it seems likely that both *cis* and *trans* isomers would have some existence in solution. The spectroscopic absence of one isomer in both cases may come from slight, but decisive, thermodynamic preferences; alternatively, rapid intramolecular isomerization or the overlap of broad, adjacent NMR resonances could be obscuring the presence of the other isomer.

**Dinuclear Cluster Structures.** All dinuclear clusters in this study have been characterized by single-crystal X-ray diffraction analysis. Thermal ellipsoid plots are given in Figure 2 and selected metrics in Table 1.

For the [Fe<sub>2</sub>(μ–NAr)<sub>2</sub>Cl<sub>4</sub>]<sup>2–</sup> clusters (type **3**), the structures of **3a** and **3c** are known for the Li<sup>+</sup> salts;<sup>3,4a</sup> the present data with quaternary ammonium counterions are effectively equivalent to those precedent structures. Cluster **3b** was previously identified solely by its NMR spectrum,<sup>3</sup> and its crystallographic determination here confirms that earlier assignment. The structural metrics of the type **3** clusters can be compared against those of the alkylimide clusters, which are entirely new.

The near-square [Fe<sub>2</sub>(μ–NR)<sub>2</sub>]<sup>2+</sup> cores of the alkyl- and arylimide clusters are quite similar and differ noticeably only in their Fe···Fe separations, which are consistently shorter (by as much as 0.1 Å) for alkylimide species. We attribute this to the interplay of (1) the Fe–N bond length, which decreases slightly (ca. 0.02 Å) for *tert*-butylimides relative

to arylimides, and (2) the N···N separation, which remains largely invariant due, presumably, to limiting interatomic repulsion; together, these restraints force rhombic compression along the Fe···Fe axis. Experimental bond angles about the core and simple trigonometric calculations support this model. The minimization of nonbonded interatomic (Fe···Fe and N···N) repulsions also explains the perfect or near-perfect planarity of all [Fe<sub>2</sub>(μ–NR)<sub>2</sub>]<sup>2+</sup> cores studied to date. The bridging imide nitrogens are essentially planar for clusters with all-chloride (**3b**, **8**) or *trans*-oriented (**10**, **12**) terminal ligands, but pyramidalize to some extent for *cis*-ligated species (**9**, **11**); interligand steric repulsion in the *cis*-disposed clusters is the most likely cause of the nitrogen pyramidalization.

For terminal ligation, the all-chloride environments are unexceptional, while the mixed ligand sets are distinctive and uncommon. Structurally characterized examples<sup>16</sup> of amines, pyridines, or phosphines bound to tetrahedral iron are limited, particularly for the first two donor types. Existing cases occur chiefly in the Fe(II) state and are rare<sup>17,18</sup> (or nonexistent, in the case of amines) at the Fe(III) level found in the present clusters. Among these known complexes, the iron–ligand bond lengths are not strongly correlated with oxidation state but instead show high variability (sometimes exceeding 0.1 Å) within a fixed oxidation state due to the composition of the coordination sphere (e.g., due to ligand sterics, chelate constraints). Given these qualifications, the equivalent distances in complexes **9–12** are in accord with available data. The terminal amines in **9** and **12** are assigned unambiguously as neutral donors by their long Fe–N contacts in comparison to Fe–N(amide) distances (1.90–

(17) L<sub>3</sub>Fe<sup>III</sup>–N(pyridine): Fe(I)(NRAr)<sub>2</sub>(py–d<sub>5</sub>), 2.108 Å (R = C(CD<sub>3</sub>)<sub>2</sub>–Me; Ar = 2,5-C<sub>6</sub>H<sub>3</sub>FMe). Stokes, S. L.; Davis, W. M.; Odom, A. L.; Cummins, C. C. *Organometallics* **1996**, *15*, 4521.

(18) L<sub>3</sub>Fe<sup>III</sup>–PR<sub>3</sub>: (POSS)Fe(PCy<sub>3</sub>), 2.507 Å (POSS = polyhedral silsesquioxane, Cy = cyclohexyl); PhB(CH<sub>2</sub>PPh<sub>2</sub>)<sub>3</sub>Fe=N–*p*-Tol, 2.209–2.274 Å; PhB(CH<sub>2</sub>PPr<sub>2</sub>)<sub>3</sub>Fe=NAd, 2.260–2.297 Å (Ad = 1-adamantyl). (a) Liu, F.; John, K. D.; Scott, B. L.; Baker, R. T.; Ott, K. C.; Tumas, W. *Angew. Chem. Int. Ed.* **2000**, *39*, 3127. (b) Brown, S. D.; Betley, T. A.; Peters, J. C. *J. Am. Chem. Soc.* **2003**, *125*, 322. (c) Betley, T. A.; Peters, J. C. *J. Am. Chem. Soc.* **2003**, *125*, 10782.

**Table 2.** Spectroscopic Data for Dinuclear Fe–NR Clusters

cluster	$^1\text{H NMR}^a$ $\delta$ , ppm	electronic absorption <sup>b</sup> $\lambda$ , nm ( $\epsilon_M$ , $\text{L}\cdot\text{mol}^{-1}\cdot\text{cm}^{-1}$ )	Mössbauer <sup>c</sup> $\delta$ ( $ \Delta E_Q $ ), mm/s
$[\text{Fe}_2(\mu\text{-NPh})_2\text{Cl}_4]^{2-}$ ( $[\text{Et}_4\text{N}]_2\mathbf{3a}$ )	22.94 (4 H, <i>meta</i> ), –20.74 (br, 4 H, <i>ortho</i> ), –23.00 (2 H, <i>para</i> )	245 (15000), 270 (17900), 392 (5800), 455 (6600), 536 (sh, 6100), 564 (6200)	0.44 (1.17)
$[\text{Fe}_2(\mu\text{-N-}p\text{-Tol})_2\text{Cl}_4]^{2-}$ ( $[\text{Et}_4\text{N}]_2\mathbf{3b}$ )	31.22 (6 H, <i>p</i> -Me), 22.23 (4 H, <i>meta</i> ), –20.03 (br, 4 H, <i>ortho</i> )	245 (15200), 271 (17100), 397 (6000), 458 (6800), 542 (sh, 6500), 567 (6600)	
$[\text{Fe}_2(\mu\text{-NMe}_s)_2\text{Cl}_4]^{2-}$ ( $[\textit{n}\text{-Bu}_4\text{N}]_2\mathbf{3c}$ )	22.49 (4 H, <i>meta</i> ), 16.71 (6 H, <i>p</i> -Me), 13.89 (br, 12 H, <i>o</i> -Me)	268 (22400), 330 (sh, 12100), 400 (sh, 12400), 419 (15200), 593 (3400)	
$[\text{Fe}_2(\mu\text{-N}^t\text{Bu})_2\text{Cl}_4]^{2-}$ ( $[\text{Et}_4\text{N}]_2\mathbf{8}$ )	7.64 (br, 18 H)	255 (11900), 313 (sh, 6900) 350 (sh, 5300), 405 (5100), 499 (sh, 1900)	0.46 (1.55)
$\text{Fe}_2(\mu\text{-N}^t\text{Bu})_2\text{Cl}_2(\text{NH}_2^t\text{Bu})_2$ ( $\mathbf{9}$ )	7.29 (br, 18 H, imide $^t\text{Bu}$ ), 2.38 (v br, 18 H, amine $^t\text{Bu}$ )	262 (18100), 305 (sh, 8600), 350 (6000), 393 (6100), 500 (sh, 2000)	0.45 (1.49)
$\text{Fe}_2(\mu\text{-N}^t\text{Bu})_2\text{Cl}_2(\text{DMAP})_2$ ( $\mathbf{10}$ )	10.37 (4 H, <i>meta</i> ), <sup>d</sup> 7.35 (18 H, $^t\text{Bu}$ ), <sup>e</sup> 4.06 (12 H, Me <sub>2</sub> N)		
$\text{Fe}_2(\mu\text{-N}^t\text{Bu})_2\text{Cl}_2(\text{PEt}_3)_2$ ( $\mathbf{11}$ )	8.57 (br), 6.78 (br), 6.45 (br) <sup>f</sup>	263 (12400), 310 (sh, 5500), 366 (3800), 396 (3800), 513 (sh, 1300)	
$\text{Fe}_2(\mu\text{-NPh})_2\text{Cl}_2(\text{NH}_2^t\text{Bu})_2$ ( $\mathbf{12}$ )	20.47 (br, 4 H, <i>ortho</i> ), –2.74 (br, 18 H, $^t\text{Bu}$ ), –15.52 (4 H, <i>meta</i> ), –16.68 (2 H, <i>para</i> )		

<sup>a</sup> CD<sub>3</sub>CN solution, ca. 25 °C; counterion signals: Et<sub>4</sub>N<sup>+</sup>, 3.2 (q, CH<sub>2</sub>), 1.2 (t, Me); *n*-Bu<sub>4</sub>N<sup>+</sup>, 3.07 (br, CH<sub>2</sub>), 1.60 (br, CH<sub>2</sub>), 1.36 (br, CH<sub>2</sub>), 0.96 (t, Me).  
<sup>b</sup> THF solution for  $\mathbf{9}$  and  $\mathbf{11}$ , MeCN for others. <sup>c</sup> Isomer shifts measured at 4.2 K, referenced to Fe metal at room temperature; errors in fit estimated at  $\pm$  0.02 mm/s. <sup>d</sup> Ortho signal not observed. <sup>e</sup> Multiple, overlapping  $^t\text{Bu}$  signals exist in the  $\sim$ 7.35 ppm region, suggesting the existence of more than one species in solution. <sup>f</sup> Most prominent peaks; assignments unknown.

**Table 3.** Electrochemical Data<sup>a</sup> for Dinuclear Fe–NR Clusters

cluster	$E^{\text{ox}}$ , V ( $\Delta E_p$ , mV) <sup>b</sup>	$E^{\text{red}}$ , V ( $\Delta E_p$ , mV) <sup>b</sup>
A <sub>2</sub> [Fe <sub>2</sub> (μ-NR) <sub>2</sub> Cl <sub>4</sub> ]		
A = Et <sub>4</sub> N, R = Ph ( $\mathbf{3a}$ )	+0.43 (irrev)	–1.44 (irrev)
A = Et <sub>4</sub> N, R = <i>p</i> -Tol ( $\mathbf{3b}$ )	+0.38 (irrev)	–1.51 (irrev)
A = <i>n</i> -Bu <sub>4</sub> N, R = Mes ( $\mathbf{3c}$ )	+0.14 (93)	–1.65 (irrev)
A = Et <sub>4</sub> N, R = $^t\text{Bu}$ ( $\mathbf{8}$ )	+0.16 (103)	not observed
Fe <sub>2</sub> (μ-N $^t$ Bu) <sub>2</sub> Cl <sub>2</sub> X <sub>2</sub>		
X = $^t\text{BuNH}_2$ ( $\mathbf{9}$ )	+0.66 (irrev)	–1.35 (irrev)
X = PEt <sub>3</sub> ( $\mathbf{11}$ )	+0.75 (irrev)	–0.43 (irrev)

<sup>a</sup> Measured at 100 mV/s scan rate in 0.1 M (*n*-Bu<sub>4</sub>N)(ClO<sub>4</sub>)/MeCN and reported vs SCE; for [Fe<sub>2</sub>(μ-NR)<sub>2</sub>Cl<sub>4</sub>]<sup>2–</sup> clusters, chloride dissociation was suppressed using 0.1 M (*n*-Bu<sub>4</sub>N)Cl as the supporting electrolyte in the analyte solution of a dual compartment cell.<sup>3</sup> <sup>b</sup>  $E^{\text{ox/red}}$  refer to the first oxidation/reduction potentials ( $E_{1/2}$  for reversible couples,  $E_p^a$  or  $E_p^c$  for irreversible processes).

1.93 Å for  $\mathbf{1}$  and  $\mathbf{2}$ )<sup>3</sup> and by the observation and positional refinement of the amine hydrogens.

**Other Physical Properties.** Spectroscopic ( $^1\text{H NMR}$ , electronic absorption, Mössbauer) and electrochemical data for the dinuclear Fe–NR clusters are presented in Tables 2 and 3. For the arylimide species, the current data, obtained with R<sub>4</sub>N<sup>+</sup> counterions, are, as expected, essentially indistinguishable from earlier measurements made on equivalent Li<sup>+</sup> salts.<sup>3</sup> Significant  $^1\text{H NMR}$  properties have been noted in the preceding synthetic discussions; for the other measurements, we make the following specific observations:

**(a) Electronic Absorption Spectra.** The electronic spectra of the *tert*-butylimide clusters are similar overall to those of the arylimide complexes but shifted to higher energy; this behavior correlates with the trend in first ionization potential for alkyl- vs arylamines,<sup>19</sup> and we therefore attribute these features to imide-associated LMCT transitions.

**(b) Mössbauer Spectra.** The dinuclear clusters measured each exhibit single, well-resolved quadrupole doublets, with

parameters consistent for high-spin Fe(III).<sup>20</sup> The oxidation state assignment for  $\mathbf{9}$  confirms the crystallographic identification of terminal amine donors in that cluster.

**(c) Redox Behavior.** Of the dinuclear clusters examined by cyclic voltammetry, only the mesityl and *tert*-butyl derivatives  $\mathbf{3c}$  and  $\mathbf{8}$  presented reversible processes, both in the form of a single oxidative 2–/1– couple at near-identical potentials; we have previously noted the existence of this same oxidation in the voltammogram of [Li]<sub>2</sub> $\mathbf{3c}$ .<sup>3</sup> For  $\mathbf{3a}$ ,  $\mathbf{3b}$ , and  $\mathbf{9}$ , multiple, successive sweeps through their irreversible reductions eventually give rise to secondary, reversible features that seem to indicate the formation of the corresponding heterocubanes; the formation of heterocubanes by reduction of dinuclear clusters has been observed in other systems<sup>3,21</sup> and is due perhaps to the charge-facilitated lability of chloride ligands and the increased basicity of the bridging nitrogens upon reduction.

## Conclusion

The protolytic substitution of bis(trimethyl)silylamide ligands by primary amines is an effective tactic for the synthesis of Fe–NR clusters. The outcomes of these reactions, as implemented through starting complexes  $\mathbf{1}$  and  $\mathbf{2}$ , depend on a number of variables, including the nature of the amine substituent, the presence of exogenous terminal

- (19) Gas-phase first ionization energies: PhNH<sub>2</sub>, 7.7 eV;  $^t\text{BuNH}_2$ , 8.5 eV. (a) Hager, J.; Smith, M. A.; Wallace, S. C. *J. Chem. Phys.* **1985**, *83*, 4820. (b) Aue, D. H.; Webb, H. M.; Bowers, M. T. *J. Am. Chem. Soc.* **1976**, *98*, 311.
- (20) Münck, E. Aspects of <sup>57</sup>Fe Mössbauer Spectroscopy. In *Physical Methods in Bioinorganic Chemistry*; Que, L., Ed.; University Science Books: Sausalito, CA, 2000; pp 287–319. (b) Gütlich, P.; Link, R.; Trautwein, A. *Mössbauer Spectroscopy and Transition Metal Chemistry*; Springer-Verlag: Berlin, 1978.
- (21) Wong, G. B.; Bobrik, M. A.; Holm, R. H. *Inorg. Chem.* **1978**, *17*, 578.

**Table 4.** Crystallographic Data<sup>a</sup>

	[Et <sub>4</sub> N]2·PhMe	[Et <sub>4</sub> N] <sub>2</sub> 3a	[Et <sub>4</sub> N] <sub>2</sub> 3b	[ <i>n</i> -Bu <sub>4</sub> N] <sub>2</sub> 3c·4MeCN	[Fe <sub>3</sub> (μ-Cl) <sub>4</sub> (DME) <sub>5</sub> ] [7] <sub>2</sub> ·DME
formula	C <sub>27</sub> H <sub>64</sub> Cl <sub>2</sub> FeN <sub>3</sub> Si <sub>4</sub>	C <sub>28</sub> H <sub>50</sub> Cl <sub>4</sub> Fe <sub>2</sub> N <sub>4</sub>	C <sub>30</sub> H <sub>54</sub> Cl <sub>4</sub> Fe <sub>2</sub> N <sub>4</sub>	C <sub>38</sub> H <sub>106</sub> Cl <sub>4</sub> Fe <sub>2</sub> N <sub>8</sub>	C <sub>56</sub> H <sub>132</sub> Cl <sub>2</sub> Fe <sub>11</sub> N <sub>8</sub> O <sub>12</sub>
fw	669.92	696.22	724.27	1169.01	2149.45
space group	<i>P</i> 2 <sub>1</sub> / <i>n</i> (no. 14)	<i>C</i> 2/ <i>m</i> (no. 12)	<i>P</i> 2 <sub>1</sub> / <i>n</i> (no. 14)	<i>C</i> 2/ <i>c</i> (no. 15)	<i>C</i> <i>c</i> (no. 9)
<i>Z</i>	4	2	2	4	4
<i>a</i> , Å	16.379(3)	14.2101(10)	11.2513(4)	23.3740(9)	21.2691(10)
<i>b</i> , Å	11.612(2)	13.4726(11)	11.2660(5)	21.0290(9)	27.751(2)
<i>c</i> , Å	22.422(5)	9.2165(5)	14.3038(6)	16.3194(6)	19.3230(12)
β, deg	108.22(3)	107.954(4)	92.351(2)	122.2710(15)	119.177(3)
<i>V</i> , Å <sup>3</sup>	4050.7(14)	1678.5(2)	1811.58(13)	6782.4(5)	9958.0(11)
ρ <sub>calc</sub> , g/cm <sup>3</sup>	1.099	1.378	1.328	1.145	1.434
θ <sub>max</sub> , deg	24.99	26.05	26.02	22.49	21.50
total data, %	99.8	99.4	99.5	99.8	99.9
μ, mm <sup>-1</sup>	0.641	1.206	1.120	0.624	1.920
<i>R</i> <sub>1</sub> ( <i>wR</i> <sub>2</sub> ), <sup>b</sup> %	5.74 (15.79)	3.77 (8.89)	4.48 (11.11)	4.89 (12.25)	6.58 (14.44)
<i>S</i> <sup>c</sup>	1.043	1.070	1.040	1.031	1.034

	[Et <sub>4</sub> N] <sub>2</sub> 8	9·(1/3)C <sub>5</sub> H <sub>12</sub>	10·2PhMe	11	12·2THF
formula	C <sub>24</sub> H <sub>58</sub> Cl <sub>4</sub> Fe <sub>2</sub> N <sub>4</sub>	C <sub>17.67</sub> H <sub>44</sub> Cl <sub>2</sub> Fe <sub>2</sub> N <sub>4</sub>	C <sub>36</sub> H <sub>54</sub> Cl <sub>2</sub> Fe <sub>2</sub> N <sub>6</sub>	C <sub>20</sub> H <sub>48</sub> Cl <sub>2</sub> Fe <sub>2</sub> N <sub>2</sub> P <sub>2</sub>	C <sub>28</sub> H <sub>48</sub> Cl <sub>2</sub> Fe <sub>2</sub> N <sub>4</sub> O <sub>2</sub>
fw	656.24	495.17	753.45	561.14	655.30
space group	<i>P</i> 2 <sub>1</sub> / <i>n</i> (no. 14)	<i>P</i> 6 <sub>1</sub> (no. 169)	<i>P</i> 1 (no. 2)	<i>P</i> 2 <sub>1</sub> / <i>n</i> (no. 14)	<i>P</i> 2 <sub>1</sub> / <i>n</i> (no. 14)
<i>Z</i>	2	6	1	4	2
<i>a</i> , Å	12.0020(9)	19.0192(4)	9.5058(9)	8.6982(3)	10.784(2)
<i>b</i> , Å	11.5142(6)	19.0192(4)	10.6657(6)	18.3233(9)	8.840(2)
<i>c</i> , Å	12.5742(10)	12.8131(2)	11.7335(11)	18.1204(8)	17.492(4)
α, deg			70.684(5)		
β, deg	94.769(2)		68.911(4)	92.203(2)	93.63(3)
γ, deg			65.967(5)		
<i>V</i> , Å <sup>3</sup>	1731.7(2)	4013.92(13)	989.74(14)	2885.9(2)	1664.3(6)
ρ <sub>calc</sub> , g/cm <sup>3</sup>	1.259	1.229	1.264	1.292	1.308
θ <sub>max</sub> , deg	27.51	24.00	22.47	25.00	26.05
total data, %	99.4	100.0	97.9	99.8	99.7
μ, mm <sup>-1</sup>	1.165	1.292	0.899	1.311	1.061
<i>R</i> <sub>1</sub> ( <i>wR</i> <sub>2</sub> ), <sup>b</sup> %	5.64 (13.11)	4.18 (7.26)	5.00 (13.08)	4.30 (10.48)	4.67 (11.63)
<i>S</i> <sup>c</sup>	0.991	1.030	1.097	1.021	1.020

<sup>a</sup> Data collected at *T* = 200(2) K using graphite-monochromatized Mo Kα radiation ( $\lambda$  = 0.71073 Å) and  $\omega$  scans. <sup>b</sup>  $R_1 = \sum ||F_o| - |F_c|| / \sum |F_o|$ , calculated for  $I > 2\sigma(I)$ ;  $wR_2 = \{\sum [w(F_o^2 - F_c^2)^2] / \sum [w(F_o^2)^2]\}^{1/2}$ . <sup>c</sup>  $S$  = goodness of fit =  $[\sum w(F_o^2 - F_c^2)^2 / (n - p)]^{1/2}$ , where  $n$  is the number of reflections and  $p$  is the number of parameters refined.

ligands, and the identity of added counterions. The importance of these parameters has been demonstrated in the selective preparation of clusters possessing the [Fe<sub>2</sub>(μ-NR)<sub>2</sub>]<sup>2+</sup> core. We have found that, for R = aryl, the use of additional chloride ligand<sup>3</sup> and quaternary ammonium counterion is crucial in suppressing undesired redox chemistry and further cluster aggregation; for R = <sup>t</sup>Bu, excess amine can be employed to similar effect, yielding a neutral cluster (**9**) that can be transformed by ligand substitution to other dinuclear Fe–NR species; and, for successful Fe–NR cluster synthesis, the R group should be inert to β-elimination. We anticipate that the chemical controls revealed in the present study will be of general utility in future Fe–NR synthetic chemistry.

## Experimental Section

**Preparation of Compounds.** Previously reported protocols<sup>3</sup> for the manipulation of Fe–NR species, including the preparation of starting complex FeCl[N(SiMe<sub>3</sub>)<sub>2</sub>]<sub>2</sub>(THF) (**1**), were used in the present study. MeCN and HMDS (hexamethyldisiloxane) solvents were distilled from CaH<sub>2</sub> and Na metal, respectively, under pure dinitrogen atmosphere and stored over 4 Å molecular sieves. Quaternary ammonium salts were dried by two consecutive azeotropic distillations of benzene, followed by dissolution in MeCN, storage over 4 Å molecular sieves, and final recrystallization from MeCN/Et<sub>2</sub>O.

**(Et<sub>4</sub>N)[FeCl<sub>2</sub>{N(SiMe<sub>3</sub>)<sub>2</sub>}]** (**[Et<sub>4</sub>N]2**). To a solution of **1** (300 mg, 0.62 mmol) in THF (10 mL) was added (Et<sub>4</sub>N)Cl (103 mg,

0.62 mmol) suspended in THF (10 mL). The mixture was stirred for 3 h and then filtered to remove a small amount of black solid. The filtrate was concentrated in vacuo to 2 mL, diluted with pentane (10 mL), and stored at –30 °C for 1 h to give red microcrystalline material. The solid was collected (243 mg, 67% crude yield) and then recrystallized by toluene (5 mL)/*n*-pentane (20 mL) vapor diffusion. After 1 week, large red crystals, suitable for diffraction analysis,<sup>7</sup> were isolated by decantation and *n*-pentane rinse. Yield: 187 mg (77% recrystallization recovery, 52% overall yield). <sup>1</sup>H NMR (CD<sub>3</sub>CN, 25 °C) δ 1.21 (sh, 12H, CH<sub>2</sub>CH<sub>3</sub>), 3.12 (sh, 8H, CH<sub>2</sub>CH<sub>3</sub>), 9.5 (v br, 36H, SiCH<sub>3</sub>). Anal. Calcd for C<sub>20</sub>H<sub>56</sub>Cl<sub>2</sub>FeN<sub>3</sub>Si<sub>4</sub>: C, 41.58; H, 9.77; N, 7.27. Found: C, 40.73; H, 9.82; N, 6.65.

**(Et<sub>4</sub>N)<sub>2</sub>[Fe<sub>2</sub>(μ-NPh)<sub>2</sub>Cl<sub>4</sub>] (**[Et<sub>4</sub>N]<sub>2</sub>3a**). A mixture of **1** (968 mg, 2.0 mmol) and (Et<sub>4</sub>N)Cl (332 mg, 2.0 mmol) in MeCN (25 mL) was stirred for 3 h to produce an orange-red solution. Neat PhNH<sub>2</sub> (0.185 mL, 2.0 mmol) was added via syringe. The solution was stirred for 20 h, gradually developing a brown color after the first few hours that eventually became purple-brown with visible precipitate. Et<sub>2</sub>O (10 mL) was added, and the solution held at –30 °C for 24 h to yield purple-black microcrystalline product that was isolated by filtration, washed with Et<sub>2</sub>O (6 mL), and dried in vacuo for 3 h (563 mg). The filtrate was concentrated in vacuo to 5 mL, diluted with Et<sub>2</sub>O (5 mL), and stored at –30 °C for 2 d to give additional product (32 mg). Total yield: 595 mg (86%). Anal. Calcd for C<sub>28</sub>H<sub>50</sub>Cl<sub>4</sub>Fe<sub>2</sub>N<sub>4</sub>: C, 48.30; H, 7.24; N, 8.05. Found: C, 48.39; H, 7.24; N, 7.90.**

**(Et<sub>4</sub>N)<sub>2</sub>[Fe<sub>2</sub>(μ-N-*p*-Tol)<sub>2</sub>Cl<sub>4</sub>] (**[Et<sub>4</sub>N]<sub>2</sub>3b**). A mixture of **1** (484 mg, 1.0 mmol) and (Et<sub>4</sub>N)Cl (183 mg, 1.1 mmol) in THF (40 mL) was stirred for 2 h to produce an orange-red solution. Neat**

*p*-TolNH<sub>2</sub> (107 mg, 1.0 mmol) was added via syringe. The solution, which developed a brown color within 2 min, was allowed to stir for 12 h, after which time a significant quantity of purplish-black precipitate was evident. The slurry was filtered, and the collected material was washed with THF until the rinses were nearly colorless (~5 mL). The solid (260 mg) was recrystallized from 20 mL of MeCN at -30 °C to afford microcrystalline product, which was isolated by filtration and washed with MeCN (1 mL) and Et<sub>2</sub>O (1 mL). Yield: 115 mg (32%). Anal. Calcd for C<sub>30</sub>H<sub>54</sub>Cl<sub>4</sub>Fe<sub>2</sub>N<sub>4</sub>: C, 49.75; H, 7.52; N, 7.74. Found: C, 49.58; H, 7.56; N, 7.50.

**(*n*-Bu<sub>4</sub>N)<sub>2</sub>[Fe<sub>2</sub>( $\mu$ -NMe<sub>2</sub>)<sub>2</sub>Cl<sub>4</sub>] [(*n*-Bu<sub>4</sub>N)<sub>2</sub>3c]**. A mixture of **1** (968 mg, 2.0 mmol) and (*n*-Bu<sub>4</sub>N)Cl (282 mg, 2.0 mmol) in MeCN (30 mL) was stirred for 3 h to produce an orange-red solution. Neat MesNH<sub>2</sub> (0.282 mL, 2.0 mmol) was added via syringe, resulting in a slow solution color change, first to light brown, then to dark green, over the course of several hours. The solution was stirred for 24 h, then treated with Et<sub>2</sub>O (15 mL), and cooled to -30 °C to give large, dark green crystals, which were isolated by filtration, rinsed with Et<sub>2</sub>O (3 × 2 mL), and dried in vacuo for 2 h (588 mg). Concentration of the filtrate to ~10 mL, addition of Et<sub>2</sub>O (5 mL), and cooling to -30 °C produced a second crop of crystalline product (160 mg). Total yield: 748 mg (74%). Anal. Calcd for C<sub>50</sub>H<sub>94</sub>Cl<sub>4</sub>Fe<sub>2</sub>N<sub>4</sub>: C, 59.77; H, 9.43; N, 5.58. Found: C, 59.78; H, 10.08; N, 5.44.

**Fe<sub>2</sub>( $\mu_3$ -N<sup>t</sup>Bu)<sub>4</sub>Cl<sub>4</sub> (**6**)**. To a stirred, dark red solution of **1** (1.937 g, 4.0 mmol) in THF (25 mL) was added neat <sup>t</sup>BuNH<sub>2</sub> (0.42 mL, 4.0 mmol) via gastight syringe. Within 15 min, the solution color began to change to dark brown. The reaction was allowed to stir at room temperature for 6 h, then filtered, evaporated to a dark brown glass (~6 h in vacuo), and extracted with 40 mL of *n*-pentane (in portions; to minimize the dissolution of contaminating species, the extraction was not exhaustive, and the final pentane wash was still dark in color). The dark brown filtrate was evaporated to dryness (~130 mg), redissolved in benzene (10 mL), filtered, and concentrated to ~4 mL. Evaporative diffusion with HMDS at room temperature for 2 d afforded crystals of **6**, which were isolated, rinsed with cold HMDS (1 mL), and dried under nitrogen flow for 20 min. Yield: 78 mg (12%). Compound identity was established by <sup>1</sup>H NMR and crystallographic analysis.<sup>2</sup> Anal. Calcd for C<sub>16</sub>H<sub>36</sub>Cl<sub>4</sub>Fe<sub>2</sub>N<sub>4</sub>: C, 29.58; H, 5.58; N, 8.62. Found: C, 29.90; H, 5.82; N, 8.29. LDI-MS: 649.1 (Theory: 649.7).

**[Fe<sub>3</sub>( $\mu$ -Cl)<sub>4</sub>(DME)<sub>5</sub>][Fe<sub>4</sub>( $\mu_3$ -N<sup>t</sup>Bu)<sub>4</sub>Cl<sub>4</sub>]<sub>2</sub> [(Fe<sub>3</sub>( $\mu$ -Cl)<sub>4</sub>(DME)<sub>5</sub>]-[7]<sub>2</sub>**. To a stirred, dark red solution of **1** (1.937 g, 4.0 mmol) in THF (25 mL) was added a solution of <sup>t</sup>BuNH<sub>2</sub> (0.293 g, 4.0 mmol) in THF (5 mL), followed by an additional 20 mL of THF. The dark red solution was heated to 80 °C for 12 h, then allowed to cool to room temperature, filtered, and evaporated to dryness in vacuo. The residue was rinsed with *n*-pentane until the washings were clear, and the resulting gray-black solid was dried under nitrogen flow for 20 min. This solid contained monoanionic cluster **7** as the only significant Fe-NR product by <sup>1</sup>H NMR assay.<sup>14</sup> Although we were unable to obtain analytically pure **7** from this system, storage of a concentrated DME solution of this material at -30 °C provided single crystals of [Fe<sub>3</sub>( $\mu$ -Cl)<sub>4</sub>(DME)<sub>5</sub>][7]<sub>2</sub>·DME for diffraction analysis.<sup>13</sup>

**(Et<sub>4</sub>N)<sub>2</sub>[Fe<sub>2</sub>( $\mu$ -N<sup>t</sup>Bu)<sub>2</sub>Cl<sub>4</sub>] [(Et<sub>4</sub>N)<sub>2</sub>8]**. A solution of (Et<sub>4</sub>N)Cl (66 mg, 0.4 mmol) in MeCN (4 mL) was added to a stirred, dark orange-black solution of **9** (94 mg, 0.2 mmol) in MeCN (10 mL). After 2 h, the color had changed to a deeper brown. The solution was evaporated to dryness in vacuo (3 h), and the residue was dissolved in a minimal amount of MeCN (4 mL). Diffusion of Et<sub>2</sub>O into this solution at -30 °C for 5 d gave microcrystalline (Et<sub>4</sub>N)<sub>2</sub>8 (74 mg). A second crop of crystals was obtained by volume

reduction (to 2 mL) and further diffusion of Et<sub>2</sub>O at -30 °C for 5 d (33 mg). Total yield: 107 mg (81%). Anal. Calcd for C<sub>24</sub>H<sub>58</sub>Cl<sub>4</sub>Fe<sub>2</sub>N<sub>4</sub>: C, 43.90; H, 8.91; N, 8.54. Found: C, 43.95; H, 8.86; N, 8.45.

**Fe<sub>2</sub>( $\mu$ -N<sup>t</sup>Bu)<sub>2</sub>Cl<sub>2</sub>(NH<sub>2</sub><sup>t</sup>Bu)<sub>2</sub> (**9**)**. A dark red solution of **1** (1.937 g, 4.0 mmol) in THF (30 mL) was treated with neat <sup>t</sup>BuNH<sub>2</sub> (1.68 mL, 16 mmol), which deepened the solution color to red-brown within minutes. The reaction was stirred for 9 h, evaporated in vacuo, and washed with *n*-pentane (40 mL) to afford a rust-colored solid. This material was dissolved in THF (30 mL), charged with *n*-pentane (15 mL), concentrated, and held at -30 °C for 2 d to yield microcrystalline **9**, which was isolated by filtration and dried in vacuo (218 mg). A second crop of **9** was obtained by volume reduction of the filtrate to incipient crystallization, cooling to -30 °C, and diffusion of pentane (294 mg). Total yield: 512 mg (54%). Anal. Calcd for C<sub>16</sub>H<sub>40</sub>Cl<sub>2</sub>Fe<sub>2</sub>N<sub>4</sub>: C, 40.79; H, 8.56; N, 11.89. Found: C, 41.00; H, 8.08; N, 11.51.

**Fe<sub>2</sub>( $\mu$ -N<sup>t</sup>Bu)<sub>2</sub>Cl<sub>2</sub>(DMAP)<sub>2</sub> (**10**)**. A solution of 4-dimethylaminopyridine (DMAP, 0.049 g, 0.40 mmol) in THF (2 mL) was added to a solution of **9** (0.094 g, 0.20 mmol) in THF (10 mL), and the resulting solution was stirred for 24 h. The orange-black solution was filtered to isolate crude **10**, dried in vacuo to ensure complete removal of THF solvent, then washed with *n*-pentane (20 mL), and dried again. Diffraction-quality crystals of **10**·2PhMe were grown by storage of a concentrated toluene solution of this solid at -30 °C; as discussed in the main text, efforts to obtain analytically pure **10** in bulk were unsuccessful.

**Fe<sub>2</sub>( $\mu$ -N<sup>t</sup>Bu)<sub>2</sub>Cl<sub>2</sub>(PEt<sub>3</sub>)<sub>2</sub> (**11**)**. To an orange-black solution of **9** (190 mg, 0.40 mmol) in MeCN (8 mL) was added PEt<sub>3</sub> (0.472 mL, 3.2 mmol), causing an immediate color change to reddish-purple. The solution was stored at -30 °C for 3 d and then filtered to isolate crystalline **11** as very long black needles. Yield: 170 mg (76%). Anal. Calcd for C<sub>20</sub>H<sub>38</sub>Cl<sub>2</sub>Fe<sub>2</sub>N<sub>2</sub>P<sub>2</sub>: C, 42.81; H, 8.62; N, 4.99. Found: C, 42.47; H, 8.32; N, 5.05.

**Fe<sub>2</sub>( $\mu$ -NPh)<sub>2</sub>Cl<sub>2</sub>(NH<sub>2</sub><sup>t</sup>Bu)<sub>2</sub> (**12**)**. Neat PhNH<sub>2</sub> (0.182 mL, 2.0 mmol) was added to a solution of **9** (0.471 g, 1.0 mmol) in THF (10 mL), instantly changing the solution color to brown-purple. The solution was stirred for 4 h and then concentrated in vacuo to ~6 mL. *n*-Pentane was diffused into the solution at -30 °C over several days to yield a purple microcrystalline product, which was collected by filtration, washed with *n*-pentane (3 × 2 mL), and dried in vacuo for 4 h (300 mg). A second crop (47 mg) was obtained by concentrating the filtrate to ~3 mL and diffusing *n*-pentane into this solution at -30 °C. Total yield: 347 mg (68%). Anal. Calcd for C<sub>20</sub>H<sub>32</sub>Cl<sub>2</sub>Fe<sub>2</sub>N<sub>4</sub>: C, 47.00; H, 6.31; N, 10.96. Found: C, 47.18; H, 6.03; N, 10.89.

**GC Analysis of Benzylamine Protolysis**. A solution of **1** (10 mg, 0.018 mmol) in MeCN (1 mL) was reacted with PhCH<sub>2</sub>NH<sub>2</sub> (1.9  $\mu$ L, 0.018 mmol) under pure N<sub>2</sub> atmosphere. After 20 h, the black-brown solution was opened to air and treated with 6 M HCl (~2–3 mL) to liberate iron-bound nitrogen ligands. The acidified solution was stirred for 1 h and then extracted with CH<sub>2</sub>Cl<sub>2</sub> (3 × 1 mL). The organic fraction was dried over anhydrous Na<sub>2</sub>SO<sub>4</sub> and then analyzed by GC (vide infra) to reveal benzaldehyde (16% yield based on PhCH<sub>2</sub>NH<sub>2</sub>) as the principal product. A further partition with CH<sub>2</sub>Cl<sub>2</sub> (2 mL) showed no remaining products extractable from the acidic phase. The aqueous fraction was then cooled in an ice bath, treated with Na<sub>2</sub>EDTA·2H<sub>2</sub>O (50 mg),<sup>22</sup> made basic to litmus with 20% NaOH, stirred vigorously for 2 h at room temperature, and extracted with CH<sub>2</sub>Cl<sub>2</sub> (3 × 1 mL). The organic fraction was dried over anhydrous Na<sub>2</sub>SO<sub>4</sub> and then analyzed by GC (vide infra) to reveal PhCH<sub>2</sub>NH<sub>2</sub> (18% recovery) as the predominant extracted component.

In control analyses (using PhCH<sub>2</sub>NH<sub>2</sub> dissolved in MeCN), the preceding acid–base partitioning protocol typically afforded ~70% maximal recoveries of amine. The total yield of nitrogen-containing species from analysis of the protolysis reaction is about half this amount. The fate of the missing organic nitrogen is unclear at present.

GC analyses were performed using an Agilent 6850A Series GC System equipped with an Agilent J&W HP-1 capillary column (dimethylpolysiloxane, 30 m length × 0.32 mm i.d. × 25 μm film) and a flame ionization detector. The injection chamber was held at 260 °C, He carrier gas was delivered at 27.71 PSI at a flow rate of 4.5 mL/min, and the column temperature was ramped at 10 °C/s for 8 min and held at 150 °C for 5 min, and then ramped at 20 °C/s for 5 min and held at 250 °C for 2 min. Products were identified by coinjection with authentic samples and quantitated by integration against benzophenone as a coinjected standard (~2–6 mg/3 mL CH<sub>2</sub>Cl<sub>2</sub> fraction).

**X-ray Crystallography.** Single crystals suitable for X-ray diffraction analysis were obtained under the following conditions: preparative recrystallization ([Et<sub>4</sub>N]2·PhMe, as dark red blocks); storage at –30 °C of MeCN ([Et<sub>4</sub>N]<sub>2</sub>3a, as dark purple needles), DME ([Fe<sub>3</sub>Cl<sub>4</sub>(DME)<sub>5</sub>][7]<sub>2</sub>·DME, as black needles), or toluene solutions (*trans*-10·2PhMe, as orange-black plates); THF/*n*-pentane vapor diffusion at –30 °C (*cis*-9·(1/3)*n*-C<sub>5</sub>H<sub>12</sub>, as dark orange needles; *trans*-12·2THF, as dark purple blocks); or MeCN/Et<sub>2</sub>O vapor diffusion at –30 °C ([Et<sub>4</sub>N]<sub>2</sub>3b, as purple-black rods; [*n*-Bu<sub>4</sub>N]<sub>2</sub>3c·4MeCN, as dark green rods; [Et<sub>4</sub>N]<sub>2</sub>8, as black plates; *cis*-11, as black rods).

General crystallographic procedures are described elsewhere.<sup>23</sup> Essential crystallographic data for compounds in this work are summarized in Table 4. Bound and/or lattice solvent molecules in [Et<sub>4</sub>N]2·PhMe, [Fe<sub>3</sub>Cl<sub>4</sub>(DME)<sub>5</sub>][7]<sub>2</sub>·DME, [Et<sub>4</sub>N]<sub>2</sub>8, and *cis*-9·(1/3)*n*-C<sub>5</sub>H<sub>12</sub>, and the iron anion of [Et<sub>4</sub>N]<sub>2</sub>3a were disordered; appropriate models and restraints were applied as required. SQUEEZE-BYPASS,<sup>24</sup> as implemented in PLATON,<sup>25</sup> was used to remove the electron density associated with the disordered solvent in [Et<sub>4</sub>N]2·PhMe and *cis*-9·(1/3)*n*-C<sub>5</sub>H<sub>12</sub>. Specific details for individual structure determinations are given as Supporting Information.

**Other Physical Measurements.** Spectroscopic (<sup>1</sup>H NMR, electronic absorption, Mössbauer) and electrochemical (cyclic voltammetry) data were obtained using protocols previously described,<sup>3</sup> with specific conditions noted in Tables 1 and 2. Elemental analyses were performed by the Microanalysis Laboratory at the School of Chemical Sciences, University of Illinois, Urbana, IL 61801 or by Oneida Research Services/Prevalere Life Sciences, Inc., Whitesboro, NY 13492.

**Acknowledgment.** We thank Dr. D. M. Ho (Princeton) for crystallographic guidance, Prof. C. Achim (Carnegie-Mellon) for helpful discussions and experimental assistance, and Prof. R. H. Holm (Harvard) for access to a Mössbauer spectrometer. The generous support of the Arnold and Mabel Beckman Foundation (Beckman Young Investigator Award) and the NSF (CAREER CHE-9984645) is gratefully acknowledged.

**Supporting Information Available:** Crystallographic data for compounds [Et<sub>4</sub>N]2·PhMe, [Et<sub>4</sub>N]<sub>2</sub>3a, [Et<sub>4</sub>N]<sub>2</sub>3b, [*n*-Bu<sub>4</sub>N]<sub>2</sub>3c·4MeCN, [Fe<sub>3</sub>Cl<sub>4</sub>(DME)<sub>5</sub>][7]<sub>2</sub>·DME, [Et<sub>4</sub>N]<sub>2</sub>8, *cis*-9·(1/3)*n*-C<sub>5</sub>H<sub>12</sub>, *trans*-10·2PhMe, *cis*-11, and *trans*-12·2THF (PDF). This material is available free of charge via the Internet at <http://pubs.acs.org>.

IC061133+

(22) The addition of EDTA prevents the formation of iron hydroxide/oxide precipitates (which interfere with the extraction of organic nitrogen-containing species) upon addition of NaOH.

(23) Kayal, A.; Ducruet, A. F.; Lee, S. C. *Inorg. Chem.* **2000**, *39*, 3696.

(24) Van der Sluis, P.; Spek, A. L. *Acta Crystallogr., Sect. A: Found. Crystallogr.* **1990**, *46*, 194.

(25) Spek, A. L. *Acta Crystallogr., Sect. A: Found. Crystallogr.* **1990**, *46*, C34.